2-1992

Measurement Of Marine Picoplankton Cell-Size By Using A Cooled, Charge-Coupled Device Camera With Image-Analyzed Fluorescence Microscopy

CL Viles
Virginia Institute of Marine Science

ME Sieracki
Virginia Institute of Marine Science

APPLIED AND ENVIRONMENTAL MICROBIOLOGY, Feb. 1992, p. 584–592
0099-2240/92/020584-09$02.00/0

Vol. 58, No. 2

Measurement of Marine Picoplankton Cell Size by Using a Cooled, Charge-Coupled Device Camera with Image-Analyzed Fluorescence Microscopy†

CHARLES L. VILES‡ AND MICHAEL E. SIERACKI§*

School of Marine Science and Virginia Institute of Marine Science, College of William and Mary, Gloucester Point, Virginia 23062

Received 9 May 1991/Accepted 19 November 1991

Accurate measurement of the biomass and size distribution of picoplankton cells (0.2 to 2.0 μm) is paramount in characterizing their contribution to the oceanic food web and global biogeochemical cycling. Image-analyzed fluorescence microscopy, usually based on video camera technology, allows detailed measurements of individual cells to be taken. The application of an imaging system employing a cooled, slow-scan charge-coupled device (CCD) camera to automated counting and sizing of individual picoplankton cells from natural marine samples is described. A slow-scan CCD-based camera was compared to a video camera and was superior for detecting and sizing very small, dim particles such as fluorochrome-stained bacteria. Several edge detection methods for accurately measuring picoplankton cells were evaluated. Standard fluorescent microspheres and a Sargasso Sea surface water picoplankton population were used in the evaluation. Global thresholding was inappropriate for these samples. Methods used previously in image analysis of nanoplankton cells (2 to 20 μm) also did not work well with the smaller picoplankton cells. A method combining an edge detector and an adaptive edge strength operator worked best for rapidly generating accurate cell sizes. A complete sample analysis of more than 1,000 cells averages about 50 min and yields size, shape, and fluorescence data for each cell. With this system, the entire size range of picoplankton can be counted and measured.

In the last 10 to 15 years, marine scientists have begun to recognize the important role that the smallest components of the plankton play in the aquatic food web and in organic- and inorganic-nutrient cycling. Concurrently, the need for faster, more accurate, and more detailed measurements of these plankton populations has increased. Nanoplankton (2 to 20 μm) and picoplankton (0.2 to 2.0 μm) are often identified and enumerated by fluorescence microscopy and visual counting (19, 20). This procedure is tedious, slow, and prone to operator error and inconsistency. It is especially difficult to measure the sizes of enough individual cells to adequately characterize population cell size distributions.

Accordingly, there has been much interest in the development of new methods and technology to automate these measurements. Two complementary technologies for rapid cell measurement have emerged: flow cytometry and image-analyzed fluorescence microscopy. Both techniques have been used with success to measure nanoplankton and autofluorescing phototrophic picoplankton (3, 22, 23, 26, 28). The ability to accurately and precisely measure the small end of the picoplankton size range, and particularly nonphotosynthetic bacteria, has proved to be problematic (18, 21). With recent advances in camera technology, we believe that image-analyzed fluorescence microscopy has good potential in this regard.

Charge-coupled device (CCD) and video cameras. Digital image analysis using video cameras has been used successfully for enumerating nanoplankton (23, 26). However, video cameras have some inherent problems that make them inappropriate for measuring cells in the 0.2- to 2-μm size fraction, a class dominated by bacteria, cyanobacteria, and small eukaryotes in aquatic environments. The fluorescence of small marine particles such as fluorochrome-stained bacteria is often at or below the noise level of video cameras, making such particles undetectable. When they are detectable, accurate sizing is difficult because of video noise. Video systems generally digitize 256 grey levels. Geometric stability, the ability of the camera to consistently sample the same spot in the scene, can also be a problem with video, especially when multiple images of the same scene are averaged to reduce noise. Nonlinearities in video camera response and analog-to-digital conversion make it difficult to compare the brightness of objects both within and between images (10).

CCD cameras perform better than video in all of the areas described above. Originally employed in astronomy (11), they have found use in basic biological and biomedical research as well (7). Because they are cooled and scan slowly, random electronic and thermal noise is essentially absent (13). As with photographic cameras, exposure times can be varied. With longer exposures (e.g., 10 s), fluorescing objects invisible to the naked eye are detectable. CCD cameras are extremely sensitive and have brightness resolution as high as 16,000 real grey levels. Geometric stability is excellent, and camera response is extremely linear.

Edge detection and cell sizing. A digital image is only an approximation of the true scene. The optics and electronics of the imaging device and the sampling process introduce errors that result in blurring. This can be partially removed by image restoration techniques that specifically account for optical blurring and sampling (6, 15). Because of blurring and

* Corresponding author.
† Virginia Institute of Marine Science contribution no. 1727.
‡ Present address: Department of Computer Science, University of Virginia, Charlottesville, VA 22903.
§ Present address: Bigelow Laboratory for Ocean Sciences, McKown Point, West Boothbay Harbor, ME 04575.

sampling, image edges are represented as areas of brightness gradient rather than exact locations. True "step" edges are rarely found in images of the real world.

Accurate sizing of marine picoplankton in digital images is essentially an edge detection problem, since the location of the edge determines the size of the cell. Though edge detection has been well researched, only limited work specific to sizing fluorochrome-stained picoplankton has been done. Sieracki et al. (21) described a simple image analysis system based on a video camera that yielded counts and size distributions for bacteria. They used a global grey level threshold to find edges and measure cells. The sampling interval was coarse (0.25 μm per pixel), making the detection and sizing of the smaller picoplankton problematic. Bjørnsen (2) used a smoothing filter and an edge enhancement filter for detection of bacteria. The implementation details for this method were omitted from the published report (2), however, making replication difficult.

Our current approach to sizing larger nanoplankton cells is to acquire subimages of single cells and analyze each individually (22). A histogram is calculated from the image, and a circular cell profile is built from the histogram. A threshold is then found by searching the cell profile for the maximum in the second derivative. The threshold is then applied back to the original image. The original name for this method, "MinD2" (22), is a misnomer, since it is actually the maximum in the second derivative of the cell profile that is found. Hereafter, we will refer to this method as "MaxD2."

Edge detection by linear filtering (or convolution) has not worked well with nanoplankton images, primarily because of high video noise levels and large amounts of detritus (nonliving particles that are not of interest) relative to the number of nanoplankton cells. However, linear filtering has promise with CCD images because of low noise levels and because the proportion of detrital particles is lower in picoplankton samples. Marr and Hildreth (14) presented an edge detection operator that was a digital approximation of previous models of human vision. The Marr-Hildreth operator (denoted $\nabla^2 G_\sigma$) can be thought of as a two-step convolution operation in which an image is first edge enhanced with the Laplacian

$$\nabla^2 = \frac{\partial^2}{\partial x^2} + \frac{\partial^2}{\partial y^2} \tag{1}$$

and then smoothed with the zero-mean Gaussian function

$$G_\sigma = \frac{1}{2\pi\sigma^2} \exp\left(-\frac{x^2 + y^2}{2\sigma^2}\right) \tag{2}$$

where σ is the standard deviation. Zero crossings in the output image correspond to local second-derivative maxima in the input image. Intuitively, these crossings can be thought of as areas of rapidly changing grey level in the input image. Horn (9), Gonzalez and Wintz (5), and Ballard and Brown (1) all offer excellent discussions of linear filtering theory and practice.

Van Vliet et al. (27) demonstrated an adaptive variation of the Marr-Hildreth operator that was effective with noisy images. Their algorithm was based on the detection of zero crossings in the output of a "nonlinear Laplacian filtered image." The operator yields the maximum gradient across the pixel of interest by a search in a predefined neighborhood (either circular or square) around the pixel. They also considered the use of an edge strength detector that identified edges as areas in the smoothed input image where the grey level gradient was above a specified edge strength parameter. Accurate edge detection is necessary for accurate cell sizing. Once edges are detected, the image can be segmented. Segmentation is the step in which objects of interest (e.g., cells) are separated from the background. We have used the ideas of Marr and Hildreth (14) and Van Vliet et al. (27) to define an edge detection and segmentation method that works well for images of fluorescing picoplankton.

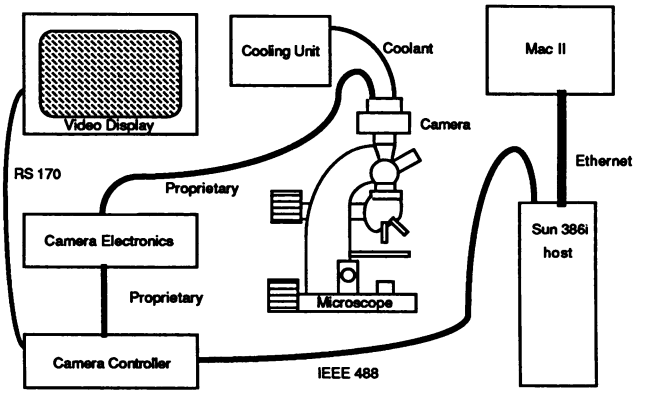

FIG. 1. Diagram of the camera and microscope system. Samples are viewed with a fluorescence microscope. Images are acquired by focusing an image and exposing the CCD chip. The camera electronics unit controls the camera and receives the image. Images are calibrated in the controller, shipped to the host computer over an IEEE 488 interface, and displayed on a separate video monitor. Through the IEEE 488, the host computer can send commands to the camera control unit and ship images back and forth. Image analysis takes place on the host computer. Summary and presentation of results are done on a Macintosh II (Mac II) connected to the host computer by Ethernet.

In this article, we describe the use of a cooled, slow-scan CCD imaging system for the measurement of picoplankton populations. We compare it with a video camera and also address some fundamental issues concerning CCD sensitivity and sampling and how these factors affect the accuracy and precision of cell counts and measurements. We then describe an edge detection and segmentation algorithm for measuring picoplankton cells. The algorithm is based on classic edge detection theory and is fast and robust.

MATERIALS AND METHODS

CCD-based image analysis system. Figure 1 is a schematic diagram of our image analysis system. We used either a Zeiss Universal or an Axioplan microscope. The camera system (Photometrics Ltd., Tucson, Ariz.) is composed of four parts, the camera head (CH220), the camera electronics unit (CE200), the camera controller (CC200), and the liquid cooling unit (LC200). The CCD (Thomson TH7882) is cooled to −40°C and has dimensions of 384 by 576 pixels, with each pixel being square and 23 μm on a side. At the highest microscope magnification (100× objective with 2× additional magnification), a square on the microscope slide that is 0.10 μm on a side is focused on each pixel on the CCD imager. Pixels are digitized to 12 bits (4,096 grey levels), and the pixel readout rate is 200 kHz. The system is controlled by a Sun 386i host computer over an IEEE 488 GPIB interface. Image calibration is performed by the camera controller. Image analysis, including segmentation, editing, and cell counting and sizing (25), is done on the host

computer. All acquisition, calibration, analysis, and display functions are initiated from window-based software on the Sun that was developed in-house and is written in the C language. Cell measurement data are generally transferred over Ethernet to a Macintosh II computer, where summation and presentation of data are done. After analysis, images can be archived or discarded.

Sample preparation. Samples for calibration of picoplankton detection and cell size were collected by bottle casts from near-surface waters in the western Sargasso Sea (35°18′N, 74°W) on a cruise on the R/V *Cape Hatteras*. Sample volumes (1 to 10 ml) were fixed with 0.3% glutaraldehyde, stained with acridine orange, and filtered onto black, 0.2-μm-pore-size Nuclepore filters (8). The stain causes bacteria to appear green or orange when excited with blue light (wavelength = 450 nm). Filters were mounted on microscope slides and covered with immersion oil and a coverslip. Picoplankton samples were either analyzed immediately aboard ship or stored frozen. Fluorescent microspheres (yellow-green; emission maximum = 540 nm; Polysciences, Inc., Warrington, Pa.) were also filtered onto black, 0.2-μm-pore-size Nuclepore filters and were analyzed immediately. Images were formed with a 100× Planapo objective with a 2× Optovar magnifier, except where noted.

Image acquisition. Picoplankton cells fluoresce green and detritus fluoresces orange and red when stained with acridine orange and excited with blue light, so we used a bandpass filter centered at 550 nm (bandwidth = 30 nm) to target the cells of interest. This step is important because the CCD is significantly more sensitive at longer wavelengths. Typical camera exposure times ranged from 4 to 8 s. To focus an image, a routine that exposed a small subregion of the CCD imager repeatedly in rapid succession (approximately twice per second) was used. Once the field was properly focused, a full-frame image was digitized, calibrated (see below), and transmitted to the host computer for analysis. Images were displayed on a video monitor, and a binary mask image representing the segmented image was displayed on the host monitor. This allowed the operator to compare segmented and unsegmented images and interactively mark unwanted objects and multiple cells.

Image calibration. Images acquired directly from the CCD camera have three undesirable components: (i) the electronic offset, or bias, of the camera; (ii) uneven brightness due to illumination of the microscope field or the optical system; and (iii) pixel-to-pixel variations in sensitivity. Before an image was analyzed, these components were removed in a calibration step called "flat fielding" (16). A bias image (dark field), b, was acquired by clearing the CCD of charge and immediately reading out an image with the camera shutter closed. A calibration image, i, represents the background illumination and was acquired by moving to a blank region on the Nuclepore filter, exciting with blue light (wavelength = 450 nm), and taking an exposure long enough to produce a mean pixel intensity, K, above 1,000. Flat fielding was performed on every pixel (x, y) in the input image, f, to produce a calibrated image, g, by using the following formula:

$$g(x, y) = \frac{[f(x, y) - b(x, y)]K}{i(x, y) - b(x, y)} \quad (3)$$

The bias and calibration images (b and i) and the scaling constant (K) were obtained for each microscope slide and used for all images acquired on that slide.

Edge detection and image segmentation. To compare methods of image segmentation, a test set of subimages of single picoplankton cells was produced by first acquiring a full image containing many picoplankton cells and then interactively selecting subimages of each individual object in the image judged to be a cell. The resulting set of 170 subimages included cells with the natural distribution of sizes and brightnesses. Using these images, we tested several edge detection and segmentation methods for their ability to detect and measure the cells. In all cases, the methods yield a binary mask image used to generate spatial measurements of each cell (area, length, width, and biovolume). The mask is applied to the original image to get brightness measurements for each cell. These are the integrated optical density (sum of the brightnesses of all the pixels making up each cell) and the average, maximum, minimum, and standard deviation of brightness for each cell. The following methods were tested.

(i) Visual thresholding. For each subimage, a threshold was chosen interactively by the operator viewing the display monitor. This threshold was used to segment the image into regions of 4 connected pixels above the threshold. These regions are considered to be cells.

(ii) Searching the cell profile for extrema in the second derivative (MaxD2 method of Sieracki et al. [22]). Segmentation was the same as in method i.

(iii) Global visual thresholding. The average of all visual thresholds (method i) was used on each individual cell subimage. Segmentation was the same as in method i.

(iv) Global MaxD2 thresholding. This method was the same as method iii, except that the average threshold of method ii was used.

(v) Marr-Hildreth method with a threshold (t) of zero ($MH_{t = 0}$). We implemented this method as two independent filters. An input image was first edge enhanced with a digital approximation of the Laplacian

$$\begin{matrix} 0 & -1 & 0 \\ -1 & 4 & -1 \\ 0 & -1 & 0 \end{matrix} \quad (4)$$

and then smoothed with a truncated Gaussian ($\sigma = 1.0$):

$$\begin{matrix} 3 & 5 & 3 \\ 5 & 8 & 5 \\ 3 & 5 & 3 \end{matrix} \quad (5)$$

The filtered image was then segmented by using a threshold of 0. The zeros in the output image correspond to the zero crossings of the second derivative.

(vi) Marr-Hildreth method at a nonzero threshold ($MH_{t \neq 0}$). This method was the same as method v, except that a positive nonzero threshold was used.

(vii) Marr-Hildreth method with edge strength (es) and thresholded at zero ($MH_{t = 0, es}$). In this method, we filtered the input image as in method v. However, the segmentation algorithm was altered to accept an edge strength parameter as well. Thus, at each candidate edge pixel above the threshold (zero in this case), the algorithm also looks at the edge strength before accepting that pixel. Edge strength is defined as the maximum gradient in the vertical and horizontal directions at the pixel of interest, $g(x, y)$:

$$es_{g(x,y)} = \max(|g(x - 1, y) - g(x, y)|, |g(x + 1, y) - g(x, y)|, |g(x, y - 1) - g(x, y)|, |g(x, y + 1) - g(x, y)|) \quad (6)$$

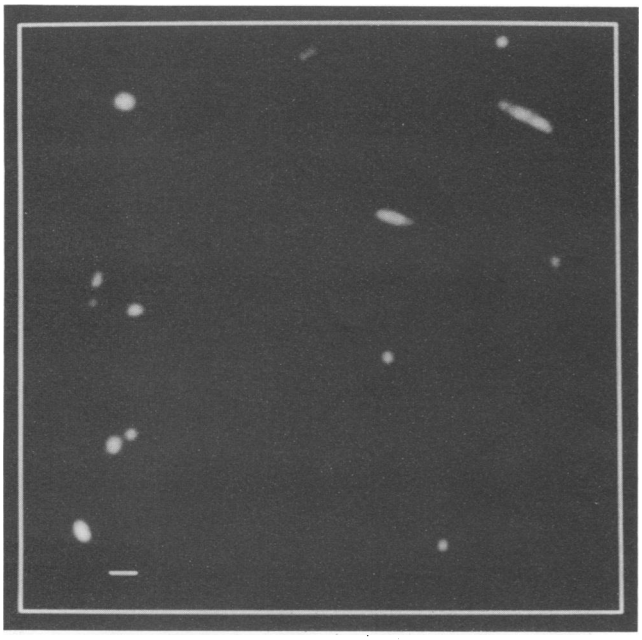

FIG. 2. A typical image of fluorochrome-stained picoplankton. Bacteria are generally small (6 to 100 pixels) and circular or oval and have a wide range of brightness and little apparent internal structure. Bar at lower left = 1 μm.

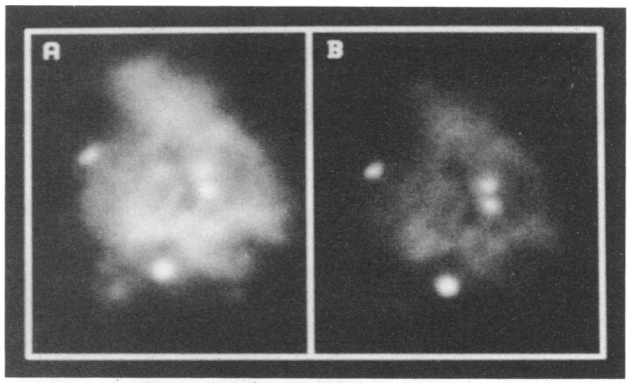

FIG. 3. The effect of using a bandpass filter is shown in an actual image of a detrital particle with bacteria on it. Images of the same scene were acquired without (A) and with (B) the filter. (A) The two discernible bright spots are bacteria and generally appear green to the human eye. Much of the detail in the center of the image is lost in amorphous material. To the eye, this material looks red and has a high degree of fluorescence in the 600- to 700-nm range. (B) The 550-nm bandpass filter eliminates the longer wavelengths, allowing better detection of the objects of interest. In this case, two more bacteria are detectable within the amorphous material. The width of the detrital particle is approximately 10 μm. The sample was taken from the Sargasso Sea in August 1990.

where g is the image resulting from the Marr-Hildreth operator. Once a pixel is accepted (i.e., above both the threshold and the required edge strength), the 4-connected region fill of the previous methods is used. Therefore, if a cell has even one accepted pixel, then the region fill is performed and the cell is counted.

In comparing methods of sizing natural picoplankton populations, we assumed that the visual thresholding method (method i) was the most accurate, so the visual sizes were used as the benchmark.

Because the true sizes of natural picoplankton cells are unknown, any sizing protocol must be tested against objects of known size. We acquired 90 images of standard fluorescent microspheres (nominal diameter = 0.98 ± 0.03 μm) with a variety of camera exposures to see how methods iii, vi, and vii performed over a range of brightness levels. These methods were selected because they all successfully ignore weak edges in an image and make no assumption about the number of objects in the image. Once the optimal method was chosen, it was used on full images containing many fluorescing objects.

RESULTS

In a typical image of marine picoplankton (Fig. 2), bacteria are generally small (6 to 100 pixels) and circular or oval, have a wide range of brightnesses, and have little internal structure when viewed by fluorescence microscopy. Brightness generally decreases monotonically from the center of the cell, and there are few areas of constant brightness. There also tends to be a fair amount of detritus that is deposited on the slide when the sample is filtered. While sometimes hard to detect visually, this detritus can have spatial scales similar to those of picoplankton and is readily detected by the CCD camera. For this reason a bandpass filter that allowed predominantly green light to pass through was used, providing good separation between cells and detritus (Fig. 3).

Low noise and high sensitivity are two of the major advantages that CCD cameras have over video cameras (Fig. 4). The mesh plots in Fig. 4 were constructed from images of the same microscope field of a sample from the Sargasso Sea taken in August 1990. The image represented in Fig. 4A was acquired with the cooled CCD system, while the image represented in Fig. 4B was acquired by averaging 16 frames from a color video camera (Sony DXC 750MD). When viewed through the microscope, two particles were visible: a fairly bright bacterium (the large peak in each plot) and an unidentified, small, dim particle (evident in the foreground in the CCD mesh plot but absent in the video mesh plot). The video image was decidedly inferior to the CCD image even after the CCD image was scaled from 12 to 8 bits for display purposes. The small, dim particle was completely lost in the video noise and was probably below the detection limit of the camera.

The problems with simple global thresholding and the ability of Laplacian-based filters to accurately find edges of both dim and bright objects in the same image are illustrated in Fig. 5. When a threshold that is appropriate for the dimmer microspheres in Fig. 5A is used, the sizes of the brighter spheres are overestimated (Fig. 5B). Similarly, a good threshold for the brighter spheres is poor for the dimmer spheres (Fig. 5C). When Fig. 5A is filtered with the Laplacian operator and thresholded at 0, both dim and bright spheres are sized accurately (Fig. 5D). Also evident in Fig. 5D is the large amount of connected background in the Laplacian-filtered image. The nominal diameter of both dim and bright microspheres was 6.1 μm.

Table 1 summarizes the results of the seven different sizing methods used on the same sample of natural bacteria. The histogram-based second-derivative method (MaxD2) performed well, detecting 100% of the cells in the image. Global thresholding, using either the average MaxD2 or the

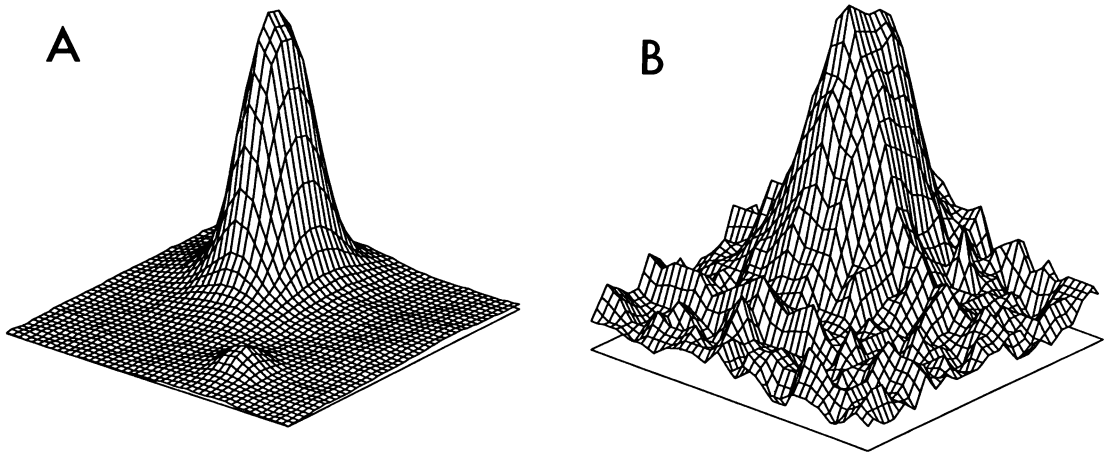

FIG. 4. Comparison of the same bacterial scene imaged by the cooled CCD camera (A) and a video camera (B). In these mesh plots, the height represents the amount of fluorescence detected. The CCD camera is able to detect small, dim particles such as that in the foreground in mesh plot A. The same particle is undetectable with the video camera (B). Because it is cooled and scans slowly, the CCD camera exhibits very little noise, in contrast to the video camera. For display purposes, the CCD image (A) has been scaled from 12 to 8 bits. The sample was taken from the Sargasso Sea in August 1990.

average visual threshold, performed poorly, missing many cells entirely and inaccurately sizing the cells that were detected. The two Marr-Hildreth methods performed best, both detecting 100% of the cells and having the lowest mean square errors.

The results from the comparison among three methods with standard microspheres are presented in Fig. 6. Each of these methods successfully ignores weak edges in the image and makes no assumptions about the number of cells in the image. The visual global threshold method yielded accurate sizes for only a very small number of spheres. The $MH_{t \neq 0}$ method worked well on all but the dimmest spheres. The $MH_{t = 0, es = 10}$ method performed best, accurately sizing microspheres at all intensities. The steps in this complete edge detection and segmentation process are illustrated in Fig. 7.

Complete analysis of a sample (>1,000 cells) takes between 35 and 90 min (mean, ca. 50 min), depending on the density of cells and detrital particles on the filter. This includes calibration, image acquisition, and analysis. Analysis yields a cell count (cells per milliliter of original sample) and measurements of the size (length, width, area, biovolume, and surface area), shape, and fluorescence intensity (minimum, maximum, average, variance, and total) of each cell. A preliminary analysis of natural picoplankton samples from the Sargasso Sea (Fig. 8) indicates that the system can

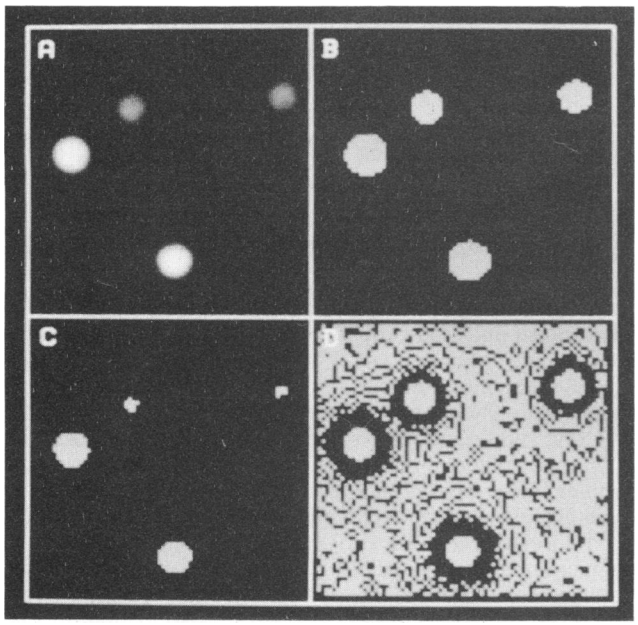

FIG. 5. The global thresholding problem is illustrated with fluorescent microspheres of similar sizes (6.1 μm in diameter) but dissimilar brightnesses (A). Choosing an optimal threshold for dim spheres causes an overestimate of the sizes of the bright spheres (B), while an optimal threshold for the bright spheres causes an underestimate of the sizes of the dim spheres (C). A Laplacian-filtered image thresholded at 0 (D) gives accurate sizes for spheres of both brightnesses. These spheres were imaged with a 16× objective and 2× additional magnification.

TABLE 1. Comparison of several edge detection methods for detecting and sizing fluorochrome-stained bacteria from Sargasso Sea surface water

Method	Type[a]	No. of bacteria detected (n = 170)	Mean area (pixels)	Mean square error[b] in area
Visual	I	170	25.1	0
Visual	G	110	63.4	11,270.0
MaxD2	I	170	21.9	182.8
MaxD2	G	109	37.7	941.6
$MH_{t = 10}$	G	170	23.3	104.0
$MH_{t = 0}$	G	170	25.0	105.7
$MH_{t = 0, es = 10}$	G	170	25.0	105.7

[a] I, method assumes that each image contains an individual cell; G, method acts on an image globally, measuring all cells in the image.

[b] Mean square error = $(1/n)\sum_{i=1}^{n} (x_i - v_i)^2$,

where x_i is the measured area of an individual cell (i) and v_i is the size determined by the visual-individual method. Only those cells that were detected by all six methods were included in the error estimate (n = 108).

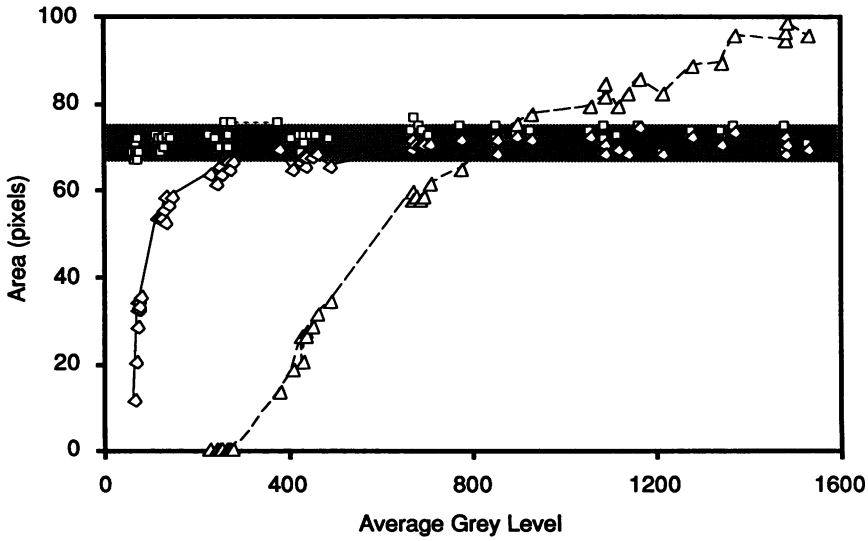

FIG. 6. Comparison of the performance of three segmentation methods using fluorescing microspheres (0.98 μm in diameter) of different brightnesses. Measured size (area) is plotted against fluorescence brightness. The visual global threshold method (triangles) performed poorly, underestimating dimmer spheres and overestimating brighter spheres. The $MH_{t=10}$ method (diamonds) accurately measured all but the very dim spheres, and the $MH_{t=0,es=10}$ method (squares) performed well at all intensities. The horizontal shaded bar represents a 95% confidence interval around the manufacturer's stated nominal microsphere size (mean = 72 pixels).

detect the full size range of the picoplankton. On the basis of size and fluorescence (data not shown) two distinct populations of particles are apparent: (i) large, bright particles which are typical bacteria (mean diameter, ca. 0.5 μm) and (ii) more abundant small, dim particles (mean diameter, ca. 0.3 μm). The large, bright objects appeared by eye to be typical oceanic bacteria, including cocci, rods, and C-shaped and sigmoid-shaped cells. The small, dim population was not so clearly bacteria. The objects in this population appeared as tiny pinpoints of orange fluorescence with no discernible morphology.

DISCUSSION

The major advantages that cooled CCD cameras have over other types of cameras are linearity, geometric stability, high brightness resolution, low noise, and high sensitivity. We found that the cooled CCD cameras can image cells that are essentially undetectable by video cameras (Fig. 4). In practice, the characteristics of these cameras that make them well suited for scientific work also cause some complications. Because of their extreme sensitivity, very faint material (e.g., a Nuclepore filter or very dim detritus) can be detected. The spectral response of CCD cameras differs from that of the human eye, so optical filters should be chosen carefully to target only the wavelengths of interest. Focusing the microscope image can be difficult, because it takes some time (3 s in our system) to acquire and display a full-frame image. There is no "live" image as there is with video cameras. This problem is alleviated by setting a subregion of the image as the focusing area and taking exposures in this region in succession while focusing. In this way, successive images can be displayed at about two or three frames per s. Also, because of the high brightness resolution, some computational tasks take longer (e.g., histogram smoothing). Fluorescence can fade over long exposures, but because of high CCD sensitivity it has not been a problem with our analyses.

As Young (29) has pointed out, the effect of image sampling on the precision of a measurement is a general phenomenon that is often overlooked or misunderstood. The position of an object in relation to a measuring grid can have a significant effect on the subsequent measurement, especially if the object is small relative to the grid. Young (29) derived an empirical formula to estimate the average error (E) associated with measuring the area of a circle randomly placed in an image:

$$E(\%) = 58.5S^{-1.6} \tag{7}$$

where

$$E(\%) = \frac{|\text{estimated area} - \text{true area}|}{\text{true area}} \times 100 \tag{8}$$

and S is samples divided by diameter. This equation shows that the precision of any measurement decreases rapidly with decreasing sample density.

In our analysis of the bacterial population shown in Fig. 8, we used a minimum size (area) of 4 pixels and did not consider any objects smaller than that. Young's formula (equation 6) yields a mean error in area due to sampling density of about 16% for an object of this size. For comparison, Estep et al. (4) used 8 pixels per circular object as a sampling density above which there was adequate measurement precision. In their system (0.16 μm per pixel in the object plane), this translates to a bacterium of about 0.5 μm in diameter with a 9% mean error in area. For our system, 4 pixels corresponds to a circle area of 0.04 μm^2 (0.23-μm diameter), and the error in area due to sampling would yield a standard deviation of about 0.008 μm^2. This value was derived by a simulation that replicated Young's (29) results. Any error in the two-dimensional image will be increased by a power of 3/2 (for a circular object) when the measurement is converted to volume.

There are two important points to make regarding sampling error and our camera system. First, the lower precision

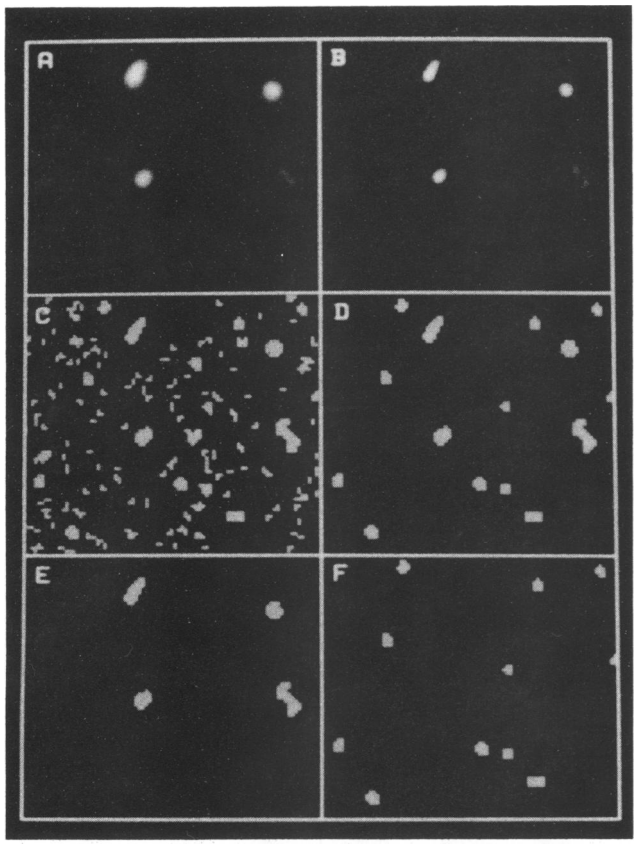

FIG. 7. Illustration of the $MH_{t=0.es}$ method. The original image (A) shows four large, bright cells as well as a number of small, dim cells. Applying a Gaussian-smoothed (σ = 1.0) Laplacian filter results in an image with highlighted edges (B). Thresholding the image at 0 shows all cells visible, as well as many other objects (C). Undesirable objects (connected background and amorphous material) can be removed (D) by applying an edge strength operator to the image in panel B, leaving only the two populations of cells. Combinations of edge strength and minimum and maximum cell sizes allow the user to target specific cell populations. For example, the bright cells can be discriminated by using an edge strength of 30 and a minimum size of 4 pixels (E). The small, dim cells are distinguished by using an edge strength of 10 and a maximum size of 15 pixels (F). The image was acquired with a 100× objective with 2.0× additional magnification. The bright cell in the upper right corner of panel A is about 1.0 μm in diameter. This sample was taken from the Sargasso Sea in August 1990.

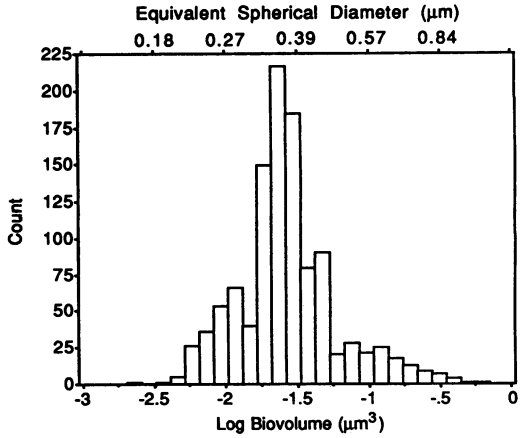

FIG. 8. Typical biovolume distribution of acridine orange-stained picoplankton-sized particles from surface Sargasso Sea water. The linear dimension of equivalent spherical diameter is also shown.

of size measurements of the smallest objects does not mean poor detection. Because of the extreme sensitivity of the camera, small cells are detected, although their measurements may be imprecise. Second, it is possible to increase the resolution of the current system so that measurement precision is increased. CCD chips with dimensions of 1,340 by 1,037 pixels and linear sample densities of 0.033 μm on the microscope slide are now commercially available. With such a camera, a 4-pixel object (with 16% error) would be equivalent to a circular diameter of 0.07 μm.

Given the characteristics of picoplankton images, an ideal edge detection and segmentation algorithm for our application would (i) find bright and dim cells in the same image, (ii) ignore weak edges that represent nonplankton material, (iii) yield accurate cell sizes, (iv) allow analysis of images with arbitrary numbers of cells present, and (v) be computationally inexpensive.

As shown in Fig. 5A, a global threshold works well only when objects of similar brightnesses are being measured. Since an optimal threshold for one sphere is suboptimal for dimmer spheres, global thresholding violates two of our main criteria: it is not accurate and may not detect bright and dim cells in the same image. A simple Laplacian filter does a good job of finding the edges of bright and dim objects. Used alone, it is not sufficient, however, since it finds many other edges as well (note the connected background in Fig. 5D).

Though the MaxD2 method performs well in sizing plankton (Table 1), it is unsatisfactory because it assumes one cell per image, as does the visual thresholding method. Single-cell acquisition is too labor-intensive to be practical for picoplankton sizing. A more desirable approach is to analyze whole images at once, forgoing this single-cell assumption so that the operator does not have to pick individual cells. In addition, the computation time of the MaxD2 method is a linear function of the brightness resolution, so going from 256 to 4,096 grey levels causes at least a 16-fold increase in execution time. The MaxD2 method is too operator and computation intensive to be practical for picoplankton images.

The Marr-Hildreth edge detector has a number of desirable properties. The Laplacian component locates the areas of maximal brightness gradient, and the Gaussian component reduces noise associated with the Laplacian component (9, 27). It detects edges regardless of their orientation in the image, and the zero crossings of the resulting image correspond to edges in the original image. Images of fluorescing circular and oval objects such as bacteria yield output images with connected, positive-valued regions surrounded by a ring of negative-valued pixels. These images are easily segmented by using a positive threshold near zero.

In our application, the simple Marr-Hildreth ($\nabla^2 G_\sigma$) operator did not suffice. In microscope images of picoplankton, weak edges that are not the particles of interest but have a spatial scale similar to the particles of interest are present. $\nabla^2 G_\sigma$ used alone finds these background edges as well as those of interest. One approach is to threshold the $\nabla^2 G_\sigma$-filtered image at some positive value. This approach would tend to eliminate objects with very weak edges. Unfortu-

nately, this leads to the problem of choosing a threshold again and is therefore undesirable.

The $MH_{t=0,es}$ method differs from that of Van Vliet et al. (27) in that the edge strength parameter is applied to the MH-filtered image rather than the original image. In a qualitative sense, using the pixel gradient at the zero crossings in the MH-filtered image as an edge strength parameter effectively goes to the edge in question and asks, "How strong is the edge?" Practically speaking, using the edge strength parameter eliminates weak background edges from the analysis. The $MH_{t=0,es}$ method satisfies all the criteria we defined above. It finds edges of both bright and dim cells, the edge strength parameter filters out weak edges, the method is accurate for both microspheres (Fig. 6) and natural samples (Table 1), and images with arbitrary numbers of cells are easily analyzed. Finally, it is computationally inexpensive, involving only two 3-by-3 convolutions followed by a scan of the convoluted image looking for edges with greater than the specified strength.

The segmentation portion of the $MH_{t=0,es}$ method (and all methods that use the Laplacian filter) assumes that a picoplankton image is essentially all edge. This assumption is reasonable for the small, brightly fluorescing cells sampled at a relatively low density (Fig. 2). Sampling at a higher rate (i.e., having more pixels make up a typical bacterium) might yield Laplacian images of picoplankton with a ring of positive values encompassed by a larger ring of negative values and having center pixels close to 0. In this case, adjustments in the algorithm would be needed in order to fill holes.

At high magnifications and low sampling densities, the effects of sampling and optical blurring may have a significant effect on cell size measurement. Our work on removing these effects at low magnifications (6) should be continued at higher magnifications. Filter kernels other than those used in this study may be more effective in edge detection in that they also address sampling and optical blurring effects (17). The extreme linearity of the sensors should allow reliable measurement of the fluorescence of individual cells in all size ranges. Because of high CCD sensitivity and the ability to take long exposures, direct measurement of small, very dim autofluorescing organisms such as the recently discovered prochlorophytes (3) may be possible.

The abundant small, dim particles detected in Sargasso Sea water (less than about 0.4 μm in linear measurement) (Fig. 8) are probably not all bacteria. This population is probably a mixture of small bacteria, viruses, and nonliving detrital particles such as those described by Koike et al. (12). A more detailed analysis of the distribution and fluorescence characteristics of these populations in the North Atlantic is described elsewhere (24).

We have presented a new image analysis system that uses fluorescence microscopy and a cooled, slow-scan CCD camera for accurate measurement of picoplankton. An adaptive variation of the Marr-Hildreth edge detector that uses an edge strength parameter similar to that described by Van Vliet et al. (27) was used successfully to segment and measure picoplankton populations. This method is unique in that it evaluates edge strength by looking at local gradients at the zero crossings in the MH-filtered image. The method is fairly robust and allows detailed analysis of natural picoplankton populations based on size and fluorescence.

ACKNOWLEDGMENTS

We thank Bob Lukens for his software development efforts, particularly in the initial interfacing stages. David A. Evans, Rajeeb Hazra, and Steven E. Reichenbach provided thoughtful comments on the manuscript.

This work was funded by NSF grant OCE-88-13356.

REFERENCES

1. **Ballard, D. H., and C. M. Brown.** 1982. Computer vision. Prentice-Hall, Inc., Englewood Cliffs, N.J.
2. **Bjørnsen, P. K.** 1986. Automatic determination of bacterioplankton biomass by image analysis. Appl. Environ. Microbiol. **51**:1199–1204.
3. **Chisholm, S., R. J. Olson, E. R. Zettler, R. Goericke, J. B. Waterbury, and N. A. Welschmeyer.** 1988. A novel free-living prochlorophyte abundant in the oceanic euphotic zone. Nature (London) **334**:340–343.
4. **Estep, K. W., F. MacIntyre, E. Hjorleifsson, and J. M. Sieburth.** 1986. MacImage: a user-friendly image-analysis system for the accurate mensuration of marine organisms. Mar. Ecol. Prog. Ser. **33**:243–253.
5. **Gonzalez, R. C., and P. Wintz.** 1987. Digital image processing. Addison-Wesley Publishing Co., Inc., Reading, Mass.
6. **Hazra, R., C. L. Viles, M. E. Sieracki, S. E. Reichenbach, and S. K. Park.** Model-based frequency response characterization of a digital image analysis system for epifluorescence microscopy. Appl. Opt., in press.
7. **Hiraoka, Y., J. W. Sedat, and D. A. Agard.** 1987. The use of a charge-coupled device for quantitative optical microscopy of biological structures. Science **238**:36–41.
8. **Hobbie, J. E., R. J. Daley, and S. Jasper.** 1977. Use of Nuclepore filters for counting bacteria by fluorescence microscopy. Appl. Environ. Microbiol. **33**:1225–1228.
9. **Horn, B. K. P.** 1986. Robot vision. MIT Press, Cambridge, Mass.
10. **Inoue, S.** 1986. Video microscopy. Plenum Press, New York.
11. **Janesick, J., and M. Blouke.** 1987. Sky on a chip: the fabulous CCD. Sky Telescope **74**:238–242.
12. **Koike, I., S. Hara, K. Terauchi, and K. Kogure.** 1990. Role of submicrometre particles in the ocean. Nature **345**:242–244.
13. **Kristian, J., and M. Blouke.** 1982. Charge-coupled devices in astronomy. Sci. Am. **247**:66–74.
14. **Marr, D., and E. C. Hildreth.** 1980. Theory of edge detection. Proc. R. Soc. Lond. B **207**:187–217.
15. **Park, S. K., and R. A. Schowengerdt.** 1982. Image sampling, reconstruction, and the effect of sample-scene phase. Appl. Opt. **21**:3142–3151.
16. **Photometrics Ltd.** 1989. Appendix B, p. 1–3. Series 200 CCD camera system user's manual. Photometrics Ltd., Tucson, Ariz.
17. **Reichenbach, S. E., S. K. Park, and R. Alter-Gartenberg.** 1990. Optimal small kernels for edge detection, p. 57–63. *In* Proceedings of the 10th International Conference on Pattern Recognition.
18. **Robertson, B. R., and D. K. Button.** 1989. Characterizing aquatic bacteria according to population, size, and apparent DNA content by flow cytometry. Cytometry **10**:70–76.
19. **Sieburth, J. M.** 1979. Sea microbes. Oxford University Press, New York.
20. **Sieburth, J. M., V. Smetacek, and J. Lenz.** 1978. Pelagic ecosystem structure: heterotrophic compartments of the plankton and their relationship to plankton size fractions. Limnol. Oceanogr. **23**:1256–1263.
21. **Sieracki, M. E., P. W. Johnson, and J. M. Sieburth.** 1985. Detection, enumeration, and sizing of planktonic bacteria by image-analyzed epifluorescence microscopy. Appl. Environ. Microbiol. **49**:799–810.
22. **Sieracki, M. E., S. E. Reichenbach, and K. L. Webb.** 1989. Evaluation of automated threshold selection methods for accurately sizing microscopic fluorescent cells by image analysis. Appl. Environ. Microbiol. **55**:2762–2772.
23. **Sieracki, M. E., P. G. Verity, and D. K. Stoecker.** Submitted for publication.
24. **Sieracki, M. E., and C. L. Viles.** Distributions and fluorochrome-staining properties of sub-micrometer particles and bacteria in the North Atlantic. Deep-Sea Res., in press.
25. **Sieracki, M. E., C. L. Viles, and K. L. Webb.** 1989. An algorithm

to estimate cell biovolume using image-analyzed microscopy. Cytometry **10**:551–557.

26. **Sieracki, M. E., and K. L. Webb.** 1991. Applications of image analyzed fluorescence microscopy for quantifying and characterizing planktonic protist communities, p. 77–100. *In* P. C. Reid, C. M. Turley, and P. H. Burkill (ed.), Protozoa and their role in marine processes. Springer-Verlag KG, Berlin.
27. **Van Vliet, L. J., I. T. Young, and G. L. Beckers.** 1989. A nonlinear Laplace operator as edge detector in noisy images. Comput. Vision Graphics Image Process. **45**:167–195.
28. **Yentsch, C. M., P. K. Horan, K. Muirhead, Q. Dortch, E. Haugen, L. Legendre, L. S. Murphy, M. J. Perry, D. A. Phinney, S. A. Pomponi, R. W. Spinrad, M. Wood, C. S. Yentsch, and B. J. Zahuranec.** 1983. Flow cytometry and cell sorting: a technique for analysis and sorting of aquatic particles. Limnol. Oceanogr. **28**:1275–1280.
29. **Young, I. T.** 1988. Sampling density and quantitative microscopy. Anal. Quant. Cytol. Histol. **10**:269–275.